Available online at www.sciencedirect.com
SCIENCE DIRECT®
Pergamon
Acta Materialia 51 (2003) 3965–3983
Acta MATERIALIA
www.actamat-journals.com

Undulation instability of a compressed elastic film on a nonlinear creeping substrate

D.S. Balint *, J.W. Hutchinson

Division of Engineering and Applied Sciences, Harvard University, 29 Oxford Street, Pierce 403, Cambridge, MA 02138, USA

Received 21 September 2002; received in revised form 16 April 2003; accepted 16 April 2003

Abstract

Undulation instabilities in a tri-layer system subject to variations of temperature are studied for the purpose of revealing a mechanism leading to the failure of thermal barrier systems. A pre-compressed oxide film with a small initial non-planarity is attached to a metal bond coat layer that is, in turn, attached to a thick superalloy substrate. The oxide film and the superalloy substrate are elastic, while the bond coat undergoes power-law creep at high temperature. The bond coat and the oxide film are subject to equi-biaxial stress changes whenever the temperature changes due to thermal mismatch with the superalloy substrate. The mismatch can be very large for some bond coat materials, such as PtNiAl, as a result of a reversible phase transformation that occurs while the temperature is changing. In the bond coat layer, the stress decays due to creep during periods at high temperature. However, during the initial stages of the decay period, the bond coat is highly susceptible to transverse deformation due to the nonlinear character of power-law creep, enabling the compressed film to undergo significant undulation growth over hundreds of thermal cycles. These periods of susceptibility appear to be a primary mechanism for undulation growth in a film that is initially nearly planar, and they explain the observation that undulation growth under cyclic temperature histories far exceeds that under isothermal conditions for the same total time exposure at high temperature. Although the behavior of the bond coat is highly nonlinear, an approximation has been developed which permits accurate description of undulation development under quite general conditions. Possibilities for reducing the susceptibility to undulation growth are discussed, as are further avenues for research.

Keywords: Thermal barrier coatings; Creep; Multi-layer thin films; High temperature deformation; Modeling

1. Introduction

Thermal barrier systems are increasingly critical to the performance of turbine engines for aircraft and power generation. The systems are designed to fulfill multiple requirements, and they are highly complex. A turbine blade system consists of an outer layer of compliant, porous zirconia (thickness≈100 μm), a film of dense aluminum oxide (thickness≈100 μm) that grows at high temperature, a metal alloy bond coat layer (thickness≈50 μm) from which the oxide film grows, and the thick superalloy blade substrate [1].

* Corresponding author. Tel.: +1-617-496-7107.
E-mail address: balint@esag.deas.harvard.edu (D.S. Balint).

1359-6454/03/$30.00 © 2003 Acta Materialia Inc. Published by Elsevier Science Ltd. All rights reserved.
doi:10.1016/S1359-6454(03)00221-0

System details, such as the specific bond coat alloy and the method used to deposit the zirconia thermal barrier, influence the durability of the multi-layer. Failures usually occur by modes such as delamination at the interface between the oxide film and the bond coat, or crack propagation in the zirconia parallel to and just outside its interface with the oxide film [2–5]. In nearly all cases, failures appear to be initiated and promoted by a non-planarity that develops in the form of undulations in the dense oxide film [6]. Research efforts have been directed at understanding the development of the undulations [5,7–12]. Understanding is clouded by the relatively large number of factors that potentially play a role in undulation development in the oxide film. These include stresses associated with growth of the oxide film, the strong temperature dependence of bond coat plasticity, the possibility of plastic yielding of the oxide film at high temperature as the growth stress increases, and thermal mismatches between components of the multi-layer system. A recent survey of attempts to model these effects is provided in [11].

One of the most striking aspects of undulation development that has been observed experimentally is the contrast between growth under cyclic temperature histories from that under isothermal histories, where, for each history, specimens experience the same total time exposure at the high temperature representative of operating conditions. Under the cyclic history, the temperature is repeatedly cycled from room temperature to the operating temperature (typically, 1150 °C or more), held for a period of time (typically on the order of 1 h) and then cooled rapidly to room temperature. In an isothermal history, the specimen is held at the operating temperature for the same total period of time but without excursions to room temperature. Far more undulation growth occurs for cyclic temperature histories, as can be seen in Fig. 1 for specimens tested by Tolpygo and Clarke [5].

The mechanics underlying undulation development has been elusive, and no clear understanding exists of the distinct difference between growth under cyclic and isothermal conditions. One study based on a spherical shell model of a well-developed undulation, concludes that the growth difference requires yielding of the oxide film to be taken into account [10]. Here, we pursue another possibility motivated by recent experimental data showing that there is an effective thermal mismatch between a PtNiAl bond coat and the superalloy substrate associated with a reversible phase

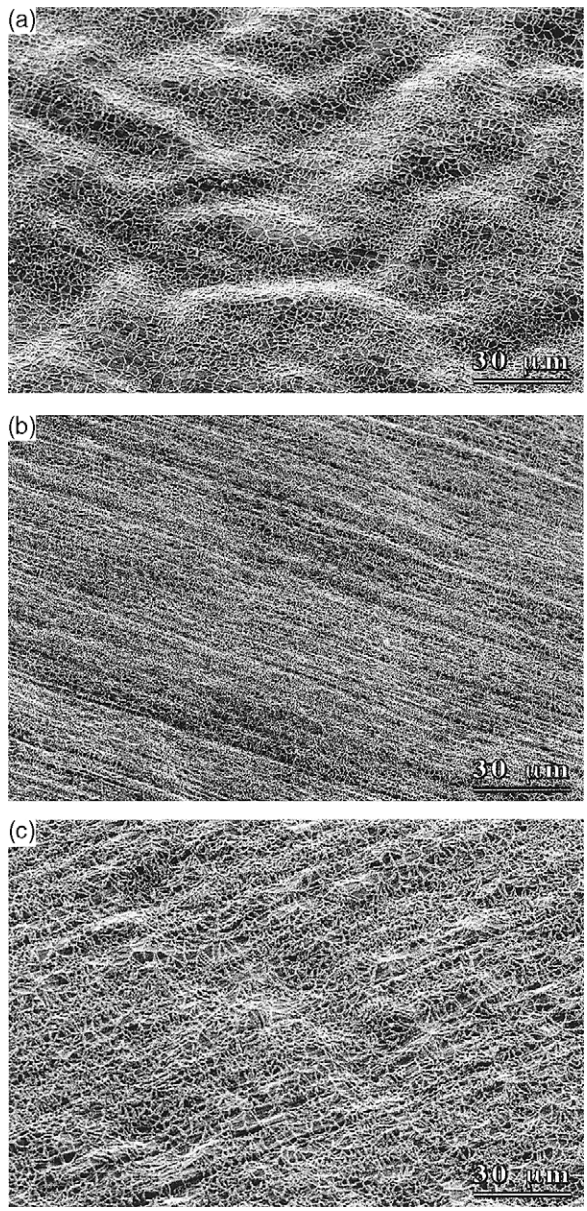

Fig. 1. Undulations in the oxide layer after (a) 100 1-h cycles, (b) 100 6-min cycles and (c) 100 h at 1150 °C under isothermal conditions. The zirconia thermal barrier is not present in this system [5].

transformation that occurs in the vicinity of 550 °C [13]. At the operating temperature, the metal bond coat has a very low effective yield strength (≈50 MPa) and undergoes power-law creep under stress. The idea underlying the present investigation is that the stress induced by the effective thermal mismatch each time the temperature is raised reduces the ability of the bond coat to resist undulation growth until the mismatch stress decays by creep. Due to the highly nonlinear character of the power-law creep of the bond coat, the mismatch stress leaves the bond coat susceptible to undulation growth driven by the compressed oxide layer. Results of the present model include the amount of undulation growth per thermal cycle, the duration of the susceptibility period, and the undulation wavelength that gives the maximum undulation growth over a typical thermal cycle. In addition, undulation growth predicted by the present model for a cyclic thermal history is compared to that of an isothermal history.

2. Model development

The objective of the present study is to elucidate a new type of instability linked to the nonlinear creep of the bond coat layer. The system isolated for investigation here is shown in Fig. 2.[1] The compliant zirconia top-layer is omitted in this study because it is not essential to the instability, although it will constrain undulation growth and must be accounted for in any attempt to model a specific thermal barrier coating system. For the same reason, normal and lateral growth of the oxide film are not included in this study. The elements of the model developed here can be used to extend the analysis to include the zirconia top-layer and growth of the oxide film.

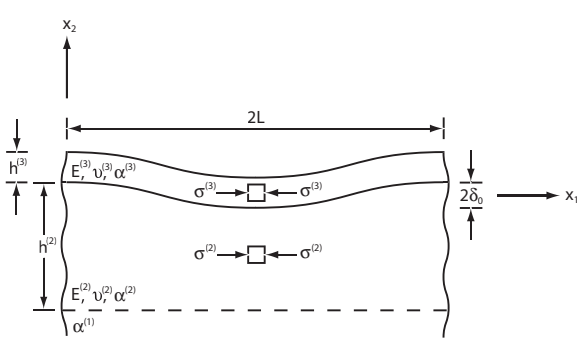

Fig. 2. A schematic showing a thin undulating elastic film on a nonlinear creeping under-layer.

[1] Layer are numbered consecutively, beginning with the substrate. Parameters are identified with their respective layers using a superscript containing the layer number in parentheses.

The system in Fig. 2 consists of the thin, elastically isotropic oxide film with Young's modulus $E^{(3)}$, Poisson's ratio $\nu^{(3)}$, coefficient of thermal expansion $\alpha^{(3)}$, and thickness $h^{(3)}$. The oxide film is assumed to have an initial sinusoidal undulation with amplitude δ_0 and half-wavelength L. Beneath the oxide film is the bond coat layer of thickness $h^{(2)}$, whose elastic properties are isotropic and given by $E^{(2)}$, $\nu^{(2)}$, and $\alpha^{(2)}$, and whose inelastic behavior is characterized by power-law creep with reference creep rate $\dot{\varepsilon}_R^{(2)}$, and reference stress $\sigma_R^{(2)}$. The total strain rate for the bond coat is given by

$$\dot{\varepsilon}_{ij}^{(2)} = \frac{1+\nu^{(2)}}{E^{(2)}}\dot{\sigma}_{ij}^{(2)} - \frac{\nu^{(2)}}{E^{(2)}}\dot{\sigma}_{kk}^{(2)}\delta_{ij} + \frac{3}{2}\dot{\varepsilon}_R^{(2)}\left(\frac{\sigma_e^{(2)}}{\sigma_R^{(2)}}\right)^{n^{(2)}-1}\frac{s_{ij}^{(2)}}{\sigma_R^{(2)}}, \quad (1)$$

where $s_{ij}^{(2)}$ is the deviatoric stress and the effective stress is

$$\sigma_e^{(2)} = \sqrt{\frac{3}{2}s_{kl}^{(2)}s_{kl}^{(2)}}. \quad (2)$$

The creep exponent, $n^{(2)}$, is typically between 3 and 5, and $\sigma_R^{(2)}$ has a strong temperature dependency.

The bi-layer is bonded to an infinitely thick, elastically isotropic substrate representing the superalloy (c.f. Fig. 2) whose coefficient of thermal expansion is $\alpha^{(1)}$. The modulus of the substrate does not come into play in the model because any lateral expansion or contraction of the substrate due to temperature change is imposed on both the oxide film and the bond coat. If the film is perfectly flat ($\delta = 0$) and the temperature is rapidly changed by ΔT uniformly throughout the multi-layer, the oxide and bond coat undergo an equi-biaxial stress change which prior to any relaxation is given by

$$\Delta\sigma_{11}^{(3)} = \Delta\sigma_{33}^{(3)} = \frac{E^{(3)}(\alpha^{(1)}-\alpha^{(3)})\Delta T}{1-\nu^{(3)}},$$
$$\Delta\sigma_{11}^{(2)} = \Delta\sigma_{33}^{(2)} = \frac{E^{(2)}(\alpha^{(1)}-\alpha^{(2)})\Delta T}{1-\nu^{(2)}}. \quad (3)$$

Stress relaxation in the bond coat occurs by creep, whether or not there is an initial undulation. Additional stress change in the elastic oxide layer occurs as the undulation grows due to a combination of bending and overall length change.

An undulation in the oxide layer in the x_2-direction gives rise to a sinusoidal normal traction at the bi-layer interface (c.f. Fig. 3) that can deform the bond coat, causing the undulation to grow if the film is under compression, as it is in the present system, or decay if the film is under tension. Provided the bond coat layer is sufficiently thick compared to the undulation half-wavelength, L, the stresses resulting from the sinusoidal traction are essentially zero at its lower boundary with the substrate. Under this circumstance, the bond coat layer thickness, $h^{(2)}$, can be taken as infinite in the determination of the undulation growth.

In the next two parts of this section, first the film and then the bond coat layer are analyzed for an applied sinusoidal normal traction with magnitude $|p|$, with the sense shown in Fig. 3, and half-wavelength L. Generalized plane strain is assumed such that there is no variation in behavior in the x_3-direction, although uniform strain changes in the x_3-direction can be accommodated. Then, in the third part, the two layers are coupled to provide the equation governing the growth of the undulation. Specific calculations are carried out in Section 3 with material properties representative of a system with a PtNiAl bond coat at 1150 °C.

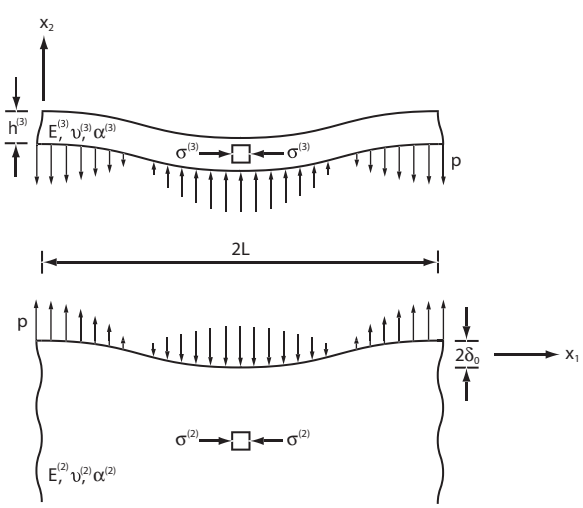

Fig. 3. A schematic showing the sinusoidal interface traction resulting from the in-plane stress in the film. Here, the underlayer is infinitely thick.

2.1. Modeling the oxide film

Let the average stress in the oxide film in the x_1-direction be given by $\sigma_{11}^{(3)} \equiv \mathrm{sgn}(\sigma_{11}^{(3)})\sigma^{(3)}$, where $\mathrm{sgn}(\sigma_{11}^{(3)}) \equiv \sigma_{11}^{(3)}/|\sigma_{11}^{(3)}|$ and $\sigma^{(3)} \equiv |\sigma_{11}^{(3)}|$. In an actual system, the stress in the oxide is compressive at the operating temperature, i.e. $\mathrm{sgn}(\sigma_{11}^{(3)}) = -1$, and its magnitude, $\sigma^{(3)}$, increases due to lateral growth of the oxide film until yielding occurs. In this paper, $\sigma^{(3)}$ will be treated as a prescribed quantity. At $t = 0$, the oxide film is assumed to have a sinusoidal shape that is given by $w_0(x_1) = \delta_0\cos(\pi x_1/L)$ for the coordinate system depicted in Fig. 2. The deflection of the film *relative to its initial shape* will be referred to as $w(x_1,t)$, so that the deflection of the film measured from the flat state at time t is $w_{\mathrm{tot}}(x_1,t) = \delta_{\mathrm{tot}}(t)\cos(\pi x_1/L)$, where the undulation amplitude is given by $\delta_{\mathrm{tot}}(t) = \delta_0 + \delta(t)$. Under the assumptions that the film is elastic, has thickness satisfying $h^{(3)} \ll L$ and the undulation slopes are not more than moderately large, i.e. $(\partial w_0/\partial x_1)^2 \ll 1$ and $(\partial w/\partial x_1)^2 \ll 1$, the oxide film shown in Fig. 2 can be modeled as a curved plate by extending von Karman theory to include the initial non-planarity, $w_0(x_1)$. This gives

$$\overline{E}^{(3)}I\frac{\partial^4 w}{\partial x_1^4} - \mathrm{sgn}(\sigma_{11}^{(3)})\sigma^{(3)}h^{(3)}\frac{\partial^2(w_0 + w)}{\partial x_1^2} = -p\cos\left(\frac{\pi x_1}{L}\right), \quad (4)$$

where $\overline{E}^{(3)} = E^{(3)}/(1-\nu^{(3)2})$, and $I = h^{(3)3}/12$ is the moment of inertia per unit depth of the film. The time dependence of the deflection arises through p which will be coupled to the creeping under-layer. A dependence of $\sigma_{11}^{(3)}$ on the average length change of the film will be included below. The separable solution to (4) is $w(x_1,t) = \delta(t)\cos(\pi x_1/L)$ where

$$\delta = \frac{p - P\delta_0}{Q}, \tag{5}$$

with

$$P = -\mathrm{sgn}(\sigma_{11}^{(3)})\frac{\sigma^{(3)}h^{(3)}\pi^2}{L^2}, \tag{6}$$

$$Q = -\frac{\sigma^{(3)}h^{(3)}\pi^2}{L^2}\left[\mathrm{sgn}(\sigma_{11}^{(3)}) + \left(\frac{L^*}{L}\right)^2\right], \tag{7}$$

$$L^* = h^{(3)}\sqrt{\frac{\pi^2\overline{E}^{(3)}}{12\sigma^{(3)}}}. \tag{8}$$

It will be seen that L^* plays a central role in establishing the critical wavelength of the undulation. Its interpretation is as follows: an infinite plate with $p = 0$ and with simple supports at equally spaced intervals of $2L^*$ will just buckle at the compressive stress $-\sigma^{(3)}$.

Within von Karman plate theory, the undulation gives an increase in the length of each periodic segment of the film, which relative to the flat state is $\frac{1}{2}\int_0^{2L}(\partial(w_0 + w)/\partial x_1)^2 \mathrm{d}x_1$. Thus, relative to the flat state, the average strain change in the film due to the undulation is $(\pi(\delta_0 + \delta)/L)^2/2$. Given an average stress $\sigma_{11}^{(3)}$ in the oxide film at an undulation amplitude of $\delta_0 + \delta$, the increment of stress resulting from an increment of growth $\Delta\delta$ is

$$\Delta\sigma_{11}^{(3)} = \frac{\overline{E}^{(3)}}{2}\left[\left(\frac{\pi(\delta_0 + \delta + \Delta\delta)}{L}\right)^2 - \left(\frac{\pi(\delta_0 + \delta)}{L}\right)^2\right] \approx \frac{\overline{E}^{(3)}\pi^2(\delta_0 + \delta)\Delta\delta}{L^2}, \tag{9}$$

assuming $|\Delta\delta/(\delta_0 + \delta)| \ll 1$ and the undulation occurs with no change in strain in the x_3-direction. As the undulation grows, the change in $\sigma_{11}^{(3)}$ can be accounted for incrementally using (9).

2.2. Modeling the bond coat/substrate system

An analytical approximation has been developed that provides an accurate representation of the response of the bond coat/substrate system when the bond coat thickness is sufficiently large relative to the undulation half-wavelength. The approximation captures the highly nonlinear interaction between the normal traction applied at the top surface of the bond coat and the equi-biaxial stress imposed by substrate strain changes. The elasticity of the bond coat layer has little direct influence on the undulation response and can be neglected. However, the elastic strains in (1) are accounted for in the bond coat stress relaxation equation, for which they are essential.

2.2.1. Analytical approximation for a thick bond coat of power-law material

Consider a bond coat layer subject to a *steadily maintained* equi-biaxial compressive stress with magnitude $\sigma^{(2)}$, i.e. $\sigma_{11}^{(2)} = \sigma_{33}^{(2)} \equiv \mathrm{sgn}(\sigma_{11}^{(2)})\sigma^{(2)} = -\sigma^{(2)}$, such that the associated effective stress is $\sigma_e^{(2)} = \sigma^{(2)}$. Superimpose onto the uniform in-plane stress state the stresses resulting from the sinusoidal traction with magnitude $|p|$ applied at the top surface of the bond coat, as shown in Fig. 3. Neglect the elastic strain rates in (1) and assume that the strain rates are given by the power-law creep contribution. If $h^{(2)}/L$ is sufficiently large compared to unity, stresses induced by p will not reach the bottom of the bond coat layer, thus it can be considered to be infinitely thick for the purpose of determining the undulation growth. From dimensional analysis and the pure power nature of the constitutive law, the solution for the rate of change of the amplitude of the undulation, $\dot{\delta}$, must have the form

$$\dot{\delta} = \dot{\varepsilon}_R^{(2)}L\left(\frac{p}{\sigma_R^{(2)}}\right)\left|\frac{p}{\sigma_R^{(2)}}\right|^{n^{(2)}-1} f\left(\left|\frac{p}{\sigma^{(2)}}\right|, n^{(2)}\right). \tag{10}$$

Because the material is nonlinear, the undulation will not have a precise sinusoidal form, even though the traction loading does. However, to a good approximation, the undulation *is* sinusoidal, with an amplitude defined as half the distance between the peak and the valley.

There are two relatively simple, well-defined limits to (10). One holds for $|p/\sigma^{(2)}| \ll 1$ such that

$$\dot{\delta} = a(n^{(2)})\dot{\varepsilon}_R^{(2)}L\left(\frac{p}{\sigma_R^{(2)}}\right)\left(\frac{\sigma^{(2)}}{\sigma_R^{(2)}}\right)^{n^{(2)}-1}. \tag{11}$$

The other holds when $|p/\sigma^{(2)}| \gg 1$ such that

$$\dot{\delta} = b(n^{(2)})\dot{\varepsilon}_R^{(2)} L \left(\frac{p}{\sigma_R^{(2)}}\right)\left|\frac{p}{\sigma_R^{(2)}}\right|^{n^{(2)}-1} . \quad (12)$$

The problem where $|p/\sigma^{(2)}|$ is small is linear in p which allows a perturbation analysis to determine the function $a(n^{(2)})$. On the other hand, the problem where $|p/\sigma^{(2)}|$ is large is inherently nonlinear in p, and thus a finite element program is needed to determine the function $b(n^{(2)})$. The solution for the coefficient $a(n^{(2)})$ is given in Appendix A and $b(n^{(2)})$ is presented in Section 2.2.2.

Finite element calculations have shown that the following interpolation of the above two limits provides an excellent approximation for $\dot{\delta}$ over the entire range of $p/\sigma^{(2)}$:

$$\dot{\delta} = L\dot{\varepsilon}_R^{(2)}\left(\frac{p}{\sigma_R^{(2)}}\right) \left[a(n^{(2)})\left(\frac{\sigma^{(2)}}{\sigma_R^{(2)}}\right)^{n^{(2)}-1} + b(n^{(2)})\left|\frac{p}{\sigma_R^{(2)}}\right|^{n^{(2)}-1}\right]. \quad (13)$$

Note that (13) depends on the magnitude of the equi-biaxial stress in the bond coat, $\sigma^{(2)}$, but not on the sign. Thus, the same expression for $\dot{\delta}$ results when the equi-biaxial stress is tensile. Furthermore, replacing $\sigma^{(2)}$ in (13) by $(\sigma_{11}^{(2)2} - \sigma_{11}^{(2)}\sigma_{33}^{(2)} + \sigma_{33}^{(2)2})^{1/2}$ gives an expression for $\dot{\delta}$ that is valid for a general biaxial stress state, which includes plane strain.[2] An example illustrating the accuracy of (13) is given in Section 2.2.2 where it is seen that the equation is accurate for $h^{(2)}/l \geq 2$. Moreover, it is shown in Section 2.3 that this equation provides a reasonably accurate approximation to the response of the bond coat even when the elastic response is included and the equi-biaxial stress is relaxing. The nonlinear coupling between the equi-biaxial stress and the normal traction arises through the first term in (13). Even at this early stage in the presentation, it can be seen that the decay of $\sigma^{(2)}$ will dramatically reduce the susceptibility of the bond coat to the normal traction imposed on it by the oxide film.

[2] The plane strain constraint $\dot{\varepsilon}_{33} = 0$ requires that $\sigma_{33} = (1/2)\sigma_{11}$ for steady-state creep.

2.2.2. Selected finite element results for the bond coat/substrate system

A finite element program has been written to model the bond coat layer of thickness $h^{(2)}$ on a very thick substrate as shown in Fig. 3. The bond coat constitutive behavior is given by (1). Eight-node generalized plane strain quadrilateral elements are used. A normal traction, $\sigma_{22}^{(2)} = p\cos(\pi x_1/L)$, $\sigma_{12}^{(2)} = 0$, is applied on the top surface. Periodic boundary conditions are imposed consistent with the in-plane symmetry of the applied traction, with in-plane and out-of-plane displacements along the bottom of the layer consistent with the uniform strains $\varepsilon_{11}^{(1)}$ and $\varepsilon_{33}^{(1)}$ imposed by the substrate. Each problem is solved incrementally in time and the geometry is updated to accommodate large deformations, although geometry changes play only a minor role for the undulation amplitudes considered in this paper. Also, the nonlinear rotation terms are included in the strain-displacement relationship which allows for moderately large rotations (c.f. Section 2.1) in a single small strain increment.

The finite element code is used for three purposes in the present paper: to compute $b(n^{(2)})$, to demonstrate the minimal influence the elastic strain contributions in the bond coat have on undulation growth, and to establish the accuracy of the nonlinear growth rate formula, (13), under a wide range of conditions. Purposes one and two are illustrated in Fig. 4. In this computation, the bond coat layer is thick ($h^{(2)}/L = 10$) and the substrate is absent, i.e. uniform strains are not imposed on the bond coat, which gives $\sigma_{11}^{(2)} = \sigma_{33}^{(2)} = 0$. At $t = 0$, the normal traction is suddenly applied on the top surface and subsequently held constant at $p/\sigma_R^{(2)} = 0.6$. The resulting undulation growth rate, $\dot{\delta}$, is plotted in Fig. 4 for several values of the creep exponent $n^{(2)}$. The undulation growth rate has a very brief transient period and then settles down to a constant value corresponding to steady-state creep of the layer. The transient corresponds to the period during which the stresses from the initial elastic response redistribute to become the steady-state creep stresses (the redistribution period is slightly longer when the biaxial stress in the bond coat is nonzero and in the process of relaxing). The transient is insignificant because the stresses from

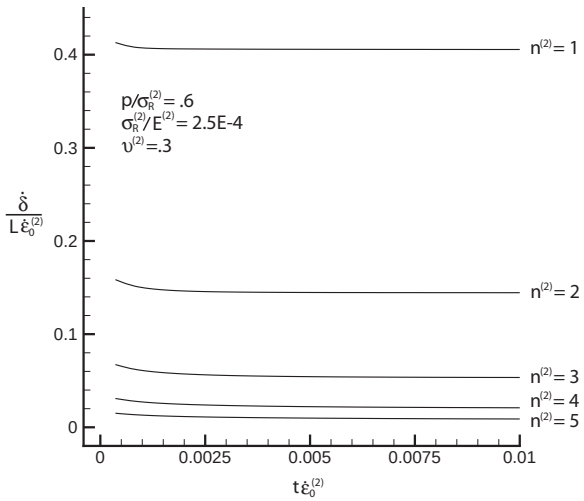

Fig. 4. Undulation growth rate determined using finite elements for a sinusoidal traction applied at the bond coat surface. In this calculation, $\sigma^{(2)}/\sigma_R^{(2)} = 0$.

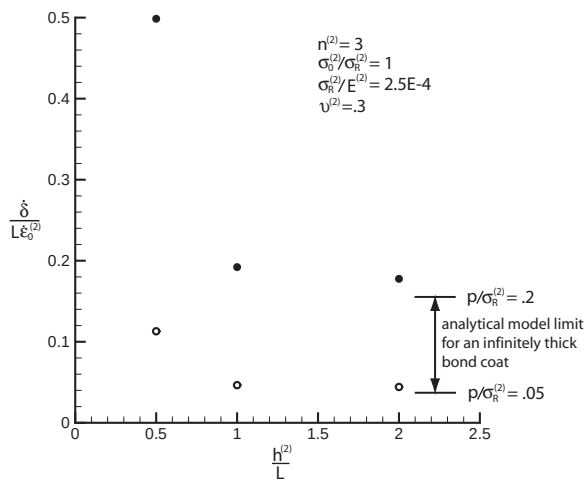

Fig. 5. Undulation growth rate under plane strain conditions determined using finite elements, including elasticity in the bond coat, for a sinusoidal traction applied at the top surface and a compressive stress applied along the right boundary, for various bond coat thicknesses, compared to the analytical formula, (13), for the infinitely thick bond coat limit. In this calculation, the compressive stress $\sigma_{11}^{(2)} \equiv -\sigma^{(2)}$ is maintained constant. The analytical formula becomes accurate when $h^{(2)}/L \geq 2$.

the elastic solution differ only slightly from the stresses predicted for power-law creep. The coefficient $b(n^{(2)})$ is obtained for each $n^{(2)}$ from (12) and the steady-state limits shown in Fig. 4. A polynomial fit to the results gives an expression that is valid for $1 \leq n^{(2)} \leq 5$:

$$b(n^{(2)}) = 1.152 - 0.6117n^{(2)} + 0.1551n^{(2)^2} - 0.02081n^{(2)^3} + 0.001170n^{(2)^4}. \quad (14)$$

The wide applicability of (13) is illustrated by the results in Fig. 5. In this example, the substrate is absent and the plane strain constraint $\varepsilon_{33}^{(2)} = 0$ is imposed. At $t = 0$, a compressive stress $\sigma_{11}^{(2)} \equiv -\sigma^{(2)}$ is applied along the right boundary and the normal traction is applied at the top surface. Both are subsequently held constant. (The finite element analysis would account for the slight perturbation about $-\sigma^{(2)}$ that would result from an initial undulation. This is ignored in the model.) The finite element simulation provides a complete analysis of the problem based on the constitutive relationship (1). The dependence of the undulation growth rate on the bond coat layer thickness relative to the half-wavelength of the surface traction is shown. Provided that $h^{(2)}/L \geq 2$, the influence of the layer thickness on the undulation growth is small. The limits shown in Fig. 5 are from (13), adjusted for plane strain by replacing $\sigma^{(2)}$ with the effective stress $\sigma_e^{(2)} = (\sqrt{3}/2)\sigma^{(2)}$, demonstrating that the interpolation is valid.[3] In Fig. 6, $\sigma_{22}^{(2)}$ stress contours are shown for the simulation in Fig. 5 corresponding to $p/\sigma_R^{(2)} = 0.2$. When $h^{(2)}/L = 2$, the stress at the lower boundary of the bond coat is small ($\sigma_{22}^{(2)}/p$ is approximately 0.05), whereas when $h^{(2)}/L = 1$, $\sigma_{22}^{(2)}/p$ is approximately 0.25. In the next subsection, a comparison is given between (13), where $\sigma^{(2)}$ is allowed to relax, and a finite element simulation.

2.3. The fully coupled system

The oxide film is coupled to the bond coat/substrate combination by eliminating p between (5) and (13) to obtain the equation governing the growth of the undulation:

$$\dot{\delta} = L\dot{\varepsilon}_R^{(2)}\left(\frac{Q\delta + P\delta_0}{\sigma_R^{(2)}}\right)\left[a(n^{(2)})\left(\frac{\sigma^{(2)}}{\sigma_R^{(2)}}\right)^{n^{(2)}-1} \quad (15)$$

[3] For plane strain, $a(3) \approx 1$.

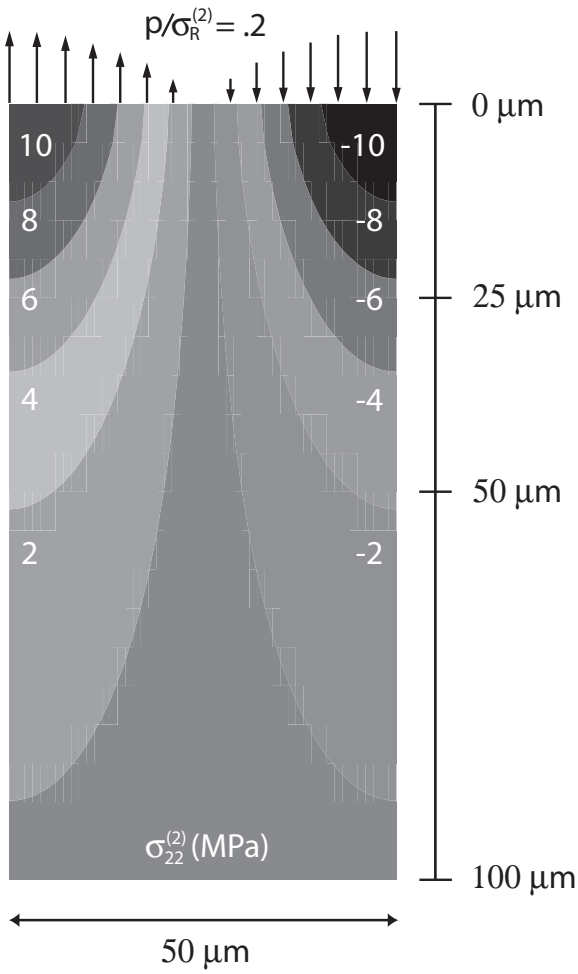

Fig. 6. Stress contours showing $\sigma_{22}^{(2)}$ for the simulation corresponding to $p/\sigma_R^{(2)} = 0.2$ in Fig. 5. The bond coat thickness is marked along the right, showing that the stress at the bottom boundary of the bond coat is very small when $h^{(2)}/L \geq 2$.

$$+ b(n^{(2)})\left|\frac{Q\delta + P\delta_0}{\sigma_R^{(2)}}\right|^{n^{(2)}-1}\Bigg].$$

The magnitude of the stress in the oxide film, $\sigma^{(3)}$, the half-wavelength of the undulation, L, and the thickness of the oxide film, $h^{(3)}$, appear in P and Q defined by (6) and (7), which have dimensions of stress/length. Appended to (15) is the equation for the creep relaxation of the equi-biaxial stress in the bond coat layer, which follows from (1) assuming the substrate is infinitely thick, i.e. $\dot{\varepsilon}_{11}^{(2)} = \dot{\varepsilon}_{33}^{(2)} = 0$,

$$\dot{\sigma}_{11}^{(2)} = -\frac{\dot{\varepsilon}_0^{(2)}E^{(2)}}{2(1-\nu^{(2)})}\left|\frac{\sigma_{11}^{(2)}}{\sigma_R^{(2)}}\right|^{n^{(2)}-1}\frac{\sigma_{11}^{(2)}}{\sigma_R^{(2)}}, \tag{16}$$

and the equation that follows from (9) for the change in the magnitude of the in-plane compressive stress in the oxide layer due to the change in its overall length:

$$\dot{\sigma}^{(3)} = \mathrm{sgn}(\sigma_{11}^{(3)})\frac{\overline{E}^{(3)}\pi^2(\delta_0 + \delta)\dot{\delta}}{L^2}. \tag{17}$$

Changes in the oxide stress from (17) are generally negligible in the early stages of growth when the undulation amplitude is very small. As mentioned earlier, changes in $\sigma^{(3)}$ and $h^{(3)}$ due to oxide growth are not considered in this paper.

A formula for the decay of the magnitude of the equi-biaxial stress in the bond coat, $\sigma^{(2)}$, can be easily derived from (16) for periods when the temperature is constant. For $n^{(2)} > 1$, given that $\sigma^{(2)} = \sigma_0^{(2)}$ at $t = 0$:

$$\frac{\sigma^{(2)}}{\sigma_0^{(2)}} = \frac{1}{[1 + t/t^*]^{1/(n^{(2)}-1)}}, \tag{18}$$

where

$$t^* = \frac{2\sigma_R^{(2)}(1-\nu^{(2)})}{(n^{(2)}-1)\dot{\varepsilon}_R^{(2)}E^{(2)}}\left(\frac{\sigma_R^{(2)}}{\sigma_0^{(2)}}\right)^{n^{(2)}-1}. \tag{19}$$

Decay of $\sigma^{(2)}$ is set by the time scale t^*, which, in turn, controls the susceptibility period for undulation growth. For values of the parameters in (19) representative of a bond coat at 1150 °C, t^* ranges from seconds to minutes.

The interpolation formula for the bond coat given by (13) is further validated by the results in Fig. 7. The system at $t = 0$ is abruptly brought up to high temperature producing an equi-biaxial compressive stress $\sigma_{11}^{(2)} = \sigma_{33}^{(2)} \equiv -\sigma^{(2)}$ in the bond coat layer (as a result of an effective thermal mismatch with the substrate), which is then allowed to relax with the substrate strains held constant (c.f. (18)), while a sinusoidal normal traction is applied at the top surface. The comparison with a full finite element analysis shows that (13) can be used with (18) to give a reasonably accurate description of

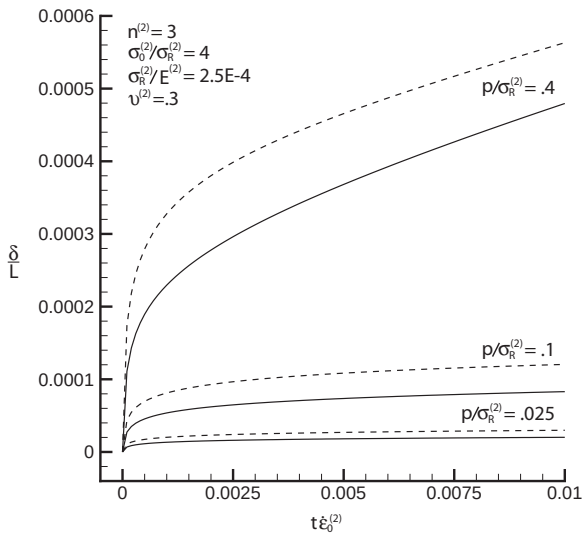

Fig. 7. Growth of the undulation for a sinusoidal traction applied at the bond coat surface and an initially stressed bond coat. The dashed line curves are based on a full finite element simulation including elasticity in the bond coat. In this calculation, $\sigma^{(2)}$ is allowed to relax.

the growth of the undulation in the bond coat surface during periods at constant temperature. Thus, while (13) was derived under conditions with $\sigma^{(2)}$ constant, it retains accuracy when $\sigma^{(2)}$ is allowed to relax. The discrepancy between the finite element and model calculations shown in Fig. 7 is primarily the effect of elasticity in the bond coat during the early stages of growth, which is neglected in the model. This does not affect the model predictions for the steady-state rate of undulation growth, which agree very well with finite element calculations provided that $p/\sigma_R^{(2)}$ is less than about 0.5.

The system of coupled, ordinary differential equations governing the undulation, (15), (17) and (18), is highly nonlinear, but it can be integrated using elementary numerical methods. When the undulation amplitude is small relative to the half-wavelength, the term in (15) that is nonlinear in the undulation amplitude can be neglected and the resulting equation is linear in δ. Accounting for the time dependence of $\sigma^{(2)}$ given by (18) and neglecting any change in $\sigma^{(3)}$, the solution to $\dot{\delta} = L\dot{\varepsilon}_R^{(2)} a(n^{(2)})(\sigma^{(2)}/\sigma_R^{(2)})^{n^{(2)}-1}(Q\delta + P\delta_0)/\sigma_R^{(2)}$ for $n^{(2)} > 1$, given that $\delta = 0$ at $t = 0$, is[4]

$$\frac{\delta}{\delta_0} = \frac{[1 + t/t^*]^{\lambda} - 1}{1 + \mathrm{sgn}(\sigma_{11}^{(3)})(L^*/L)^2}, \tag{20}$$

where $\delta = \int_0^t \dot{\delta}(\tau)\mathrm{d}\tau$ is the growth of the undulation through time t and

$$\lambda = \frac{2La(n^{(2)})Q(1-\nu^{(2)})}{(n^{(2)}-1)E^{(2)}} = -\frac{2\pi^2 a(n^{(2)})(1-\nu^{(2)})}{(n^{(2)}-1)}\frac{h^{(3)}}{L}\frac{\sigma^{(3)}}{E^{(2)}} \left[\mathrm{sgn}(\sigma_{11}^{(3)}) + t\left(\frac{L^*}{L}\right)\right]^2. \tag{21}$$

It is significant that the normalized undulation growth given by (20) depends on the bond coat stress only through the time scale t^*, and has no dependence onthe initial undulation size, $\delta_0/h^{(3)}$, although it is implicitly assumed that the undulation is small. Thus, noting that $h^{(3)}/L$ can be expressed in terms of $\sigma^{(3)}$ and L^*/L using (8), when plotted as δ/δ_0 vs. t/t^*, undulation growth given by (20) depends only on $\sigma_{11}^{(3)}$ and L^*/L.

The present system has some features in common with the behavior of a compressed elastic film on a linear visco-elastic layer [9]. Here, we have also exploited nonlinear plate theory in (4) to represent the film based on the condition $h^{(3)} \ll L$. A critical wavelength for which maximum undulation growth occurs also exists in the present system. The main difference between the present system and that with a linearly viscous under-layer is the strong coupling between the magnitude of the equibiaxial stress in the bond coat, $\sigma^{(2)}$, and the magnitude of the normal traction, $|p|$. The time-dependence of $\sigma^{(2)}$ plays the dominant role in the behavior of the present system. A second difference is that the undulation in the present system grows for all wavelengths. This is because the half-wavelength of the undulation, L, is fixed, i.e. the undulatory pattern is infinite in extent in the x_1

[4] The limit of the right hand side of (20) is well defined as $L^*/L \to 1$.

direction, therefore L cannot change, and the bond coat is modeled as a pure power-law creep material, therefore it cannot resist an applied traction. Thus, the only way for the oxide film to be relieved of some or all of its strain energy is for the undulation to grow.

3. Simulations of undulation growth

The dominant contribution to the thermal mismatch between a PtNiAl bond coat and a superalloy substrate arises from the reversible phase transformation which occurs in the bond coat in a range of temperature centered at 550 °C [13]. The transformation involves an expansion of almost 1% strain when the temperature is raised above 700 °C and a similar contraction when it is cooled below 400 °C. A schematic of the phase transformation is shown in Fig. 8. In this paper, we will not attempt to simulate the full details of the thermal cycle and the stress history in the bond coat. Instead, we note that a rapid heating of the system to the operating temperature (1150 °C) will necessarily result in an equi-biaxial compressive stress in the bond coat which is roughly its yield stress at 650 °C, since the transformation expansion far

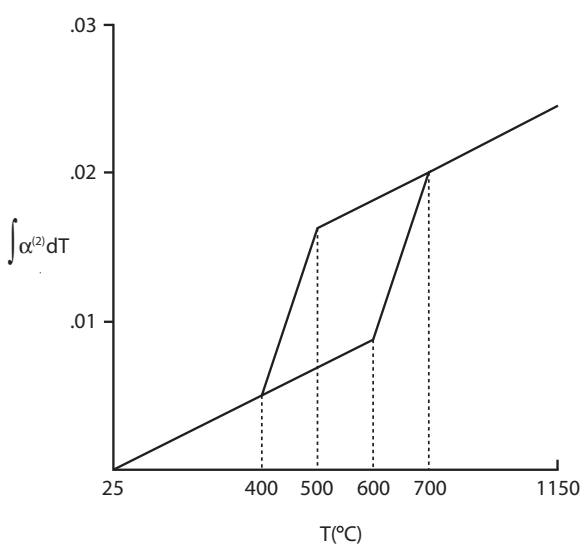

Fig. 8. A schematic of the reversible phase transformation that occurs in a PtNiAl bond coat [13].

exceeds the yield strain. Thus, at the start of the thermal cycle when the bond coat stress begins relaxing by creep, $\sigma^{(2)} = \sigma_0^{(2)}$ is expected to be on the order of the yield stress at 650 °C which the current data suggest is in the range of 200–600 MPa.

A simplified view of the stress history in the bond coat is given by the schematic shown in Fig. 9. Here, the thermal mismatch between the bond coat and the substrate, $(\alpha^{(1)}-\alpha^{(2)})$, is entirely due to the phase transformation that occurs in the bond coat. Changes in time, and temperature, are implicit in this figure. Point 1 corresponds to the start of the phase transformation during the heat-up of the first thermal cycle. The magnitude of the compressive stress increases elastically until yield occurs at point 2. During the isothermal part of the cycle, which begins at point 3, the stress in the bond coat relaxes to zero by creep. At point 4, the reverse phase transformation begins, and at point 5, the bond coat yields in tension. The clockwise circuit beginning and ending at point 6, where the system is at room temperature, gives the stress for subsequent thermal cycles. Thus, to a good approximation, the equi-biaxial compressive stress in the bond coat is renewed each time the system is heated to the operating temperature.

With $\dot{\varepsilon}_R^{(2)} = 10^{-6}\ \mathrm{s}^{-1}$, the reference stress in the creep law for the bond coat at 1150 °C, $\sigma_R^{(2)}$, is about 50 MPa. Thus, when the system reaches the operating temperature, $\sigma_0^{(2)}$ is likely to be between 4 and 10 times $\sigma_R^{(2)}$. The ratio, $\sigma_0^{(2)}/\sigma_R^{(2)}$, will be a parameter in the simulations. The simulations are based on (15) with (17) and (18) with parameter values specified in the figures which are representative of a PtNiAl system [7,13]. In the single-cycle simulations, the system is held at the operating temperature for approximately 3 h.

The rate of undulation growth at $t = 0$ is plotted as a function of $\sigma_0^{(2)}$ for several values of the initial undulation wavelength parameter, L_0^*/L, in Fig. 10. The amplitude of the undulation grows at an initial rate that is larger for smaller wavelengths, although the smaller wavelengths do not necessarily give the maximum undulation growth over time.

The growth of the undulation through time t, $\delta = \int_0^t \dot{\delta}(\tau)\mathrm{d}\tau$, is plotted as a function of time in Fig.

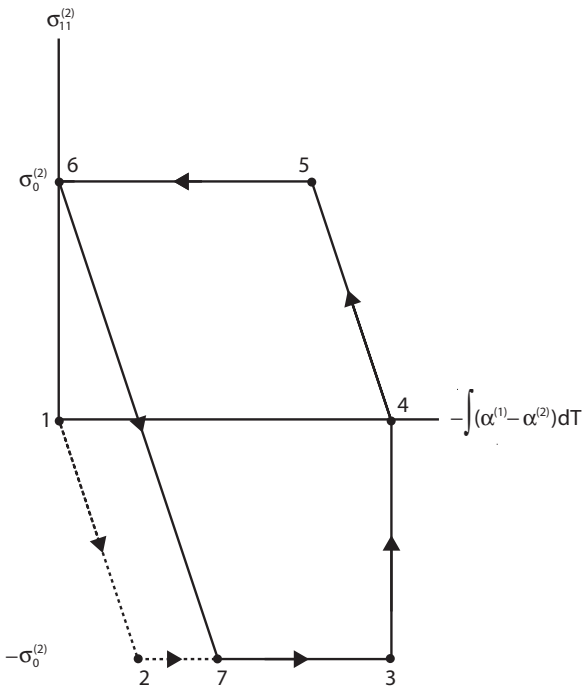

Fig. 9. A schematic of the stress history in the bond coat. The equi-biaxial compressive stress in the bond coat is renewed each time the system is heated from room temperature (point 6) to the operating temperature (point 3).

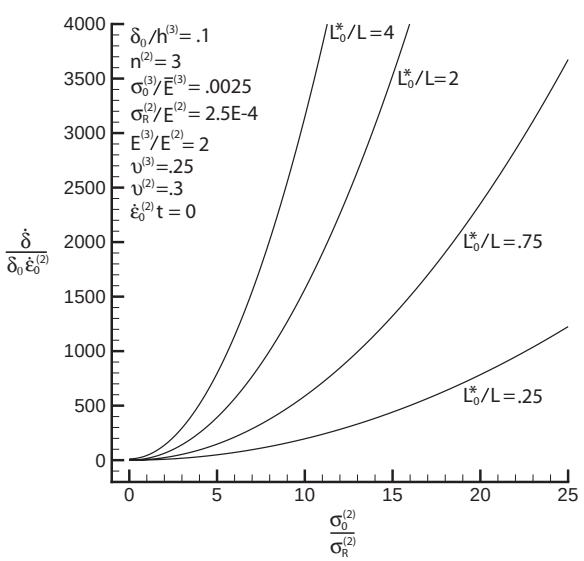

Fig. 10. Initial undulation growth rate for the fully coupled system as a function of initial bond coat stress for different undulation wavelengths.

11. Included in this plot is the history of $\sigma^{(2)}$ in the bond coat, which is given by the broad dashed line. The solid lines in this figure are based on both contributions on the right hand side of (15), while the short dashed curve, which corresponds to $L_0^*/L = 5$, neglects the contribution from the term that is nonlinear in the undulation amplitude, and the change in $\sigma^{(3)}$ from (17). The solution to the resulting approximate set of equations is given by (20). It is apparent from (20) and (19), as well as from Fig. 11, that the dominant contribution to undulation growth in the early stages arises from the interaction between $\sigma^{(2)}$ and the normal traction caused by the oxide film. It is also evident from Fig. 11 that (20) provides a good approximation of the undulation growth, although the accuracy does vary with L_0^*/L.

The qualitative aspects of undulation growth vary depending on the value of L^*/L which is evident from (15). Assuming the oxide stress is compressive, the parameter Q is non-negative when $L^*/L \leq 1$. Thus, if the system were held at the

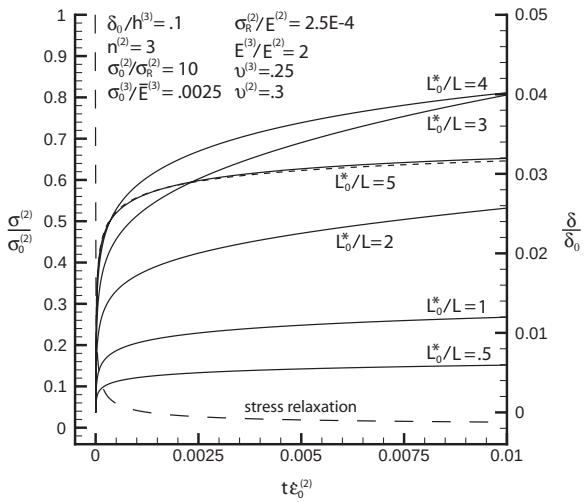

Fig. 11. Undulation growth and bond coat stress relaxation (given by the broad-dashed curve) for the fully coupled system for different undulation wavelengths. The short-dashed curve is based on (20) and corresponds to $L_0^*/L = 5$.

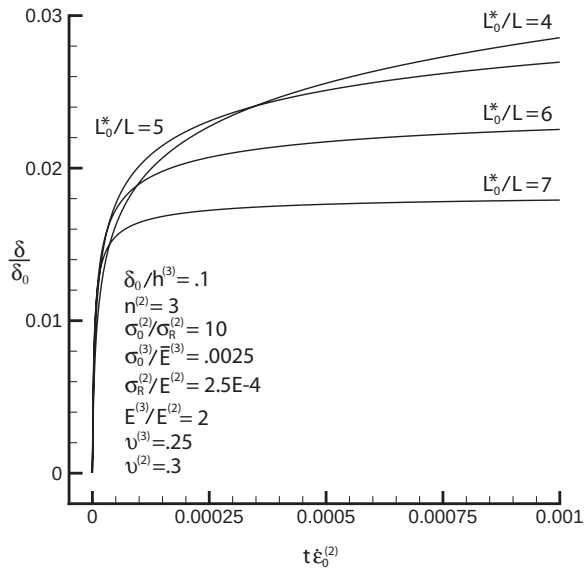

Fig. 12. Growth of the undulation for the fully coupled system for different undulation wavelengths for the period during which the undulation is highly susceptible to growth. The value of L_0^*/L that gives the quickest development of the undulation is about 4 or 5.

operating temperature indefinitely, the undulation would grow until the stress in the oxide layer was totally relaxed if $L^*/L \leq 1$, whereas the undulation would grow at a monotonically decreasing rate until growth ceased, prior to total relaxation of the oxide stress, if $L^*/L > 1$. The former situation corresponds to buckling of the oxide film. In the latter situation, equilibrium of the oxide layer is reached through a balance of the remaining strain energy stored in the oxide layer with the bending energy induced by undulation growth. A critical value of L_0^*/L exists, for which maximum undulation growth occurs over the course of a given thermal history. The critical value depends on the creep strength of the bond coat, in addition to the details of the thermal history.

A period of high susceptibility to undulation growth exists at the beginning of a thermal cycle, before the stress in the bond coat is able to relax. The period of high susceptibility is shown in Fig. 12 for various undulation wavelengths. Here, the critical value of L_0^*/L can be identified as about 4 or 5. For the parameter values used in these simulations, $L_0^*/L = 5$ corresponds to an oxide film thickness to half-wavelength ratio, $h^{(3)}/L$, of approximately 0.27.

At $t = 0$, the bond coat surface may be covered by a random roughness pattern that is made up of many undulations of differing wavelengths. Assuming all undulations are of comparable amplitude, the undulation whose wavelength is closest to the critical wavelength will reach a threshold size quickest and thereby prevent the others from developing further. This describes a process by which a fairly regular pattern, such as the one shown in Fig. 1(a), can arise from an irregular initial state.

When normalized as δ/δ_0, the undulation growth is essentially independent of $\delta_0/h^{(3)}$, as illustrated by the results in Fig. 13. Thus, the initial size of the undulation is immaterial provided it is no larger than approximately one tenth of the film thickness.

Undulation growth is plotted in Fig. 14 against t/t^* for several values of $\sigma_0^{(2)}/\sigma_R^{(2)}$. Of the two coefficients $a(n^{(2)})$ and $b(n^{(2)})$, the simple formula (20) involves only $a(n^{(2)})$, which is valid for the limit $|p/\sigma^{(2)}| \ll 1$. The prediction of the simple formula given by the dashed curve in Fig. 14 is in agreement with the curve corresponding to $\sigma_0^{(2)}/\sigma_R^{(2)} = 10$, i.e. for the initial oxide stress used in these simulations ($\sigma_0^{(3)} = 1$ GPa), which is directly related

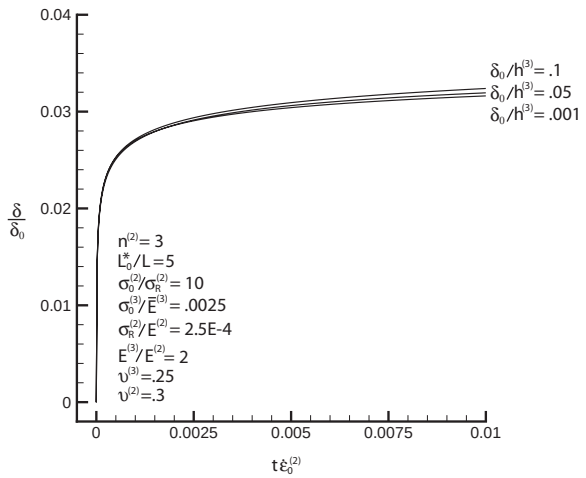

Fig. 13. Growth of the undulation for the fully coupled system for different values of the initial undulation amplitude. Undulation growth is essentially independent of the initial size of the undulation, provided it is small relative to the thickness of the oxide layer.

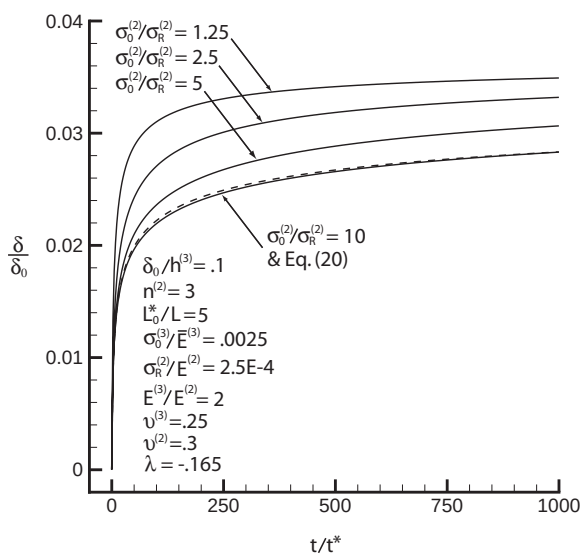

Fig. 14. Growth of the undulation vs. t/t^* for the fully coupled system for different values of the initial bond coat stress. When normalized in this manner, growth predicted by (20), which is given by the dashed curve, is independent of the bond coat stress and the initial size of the undulation. The simple Eq. (20) predicts the growth reasonably well, particularly when, in the complete simulation, the value of $\sigma_0^{(2)}/\sigma_R^{(2)}$ is 5 or larger.

to p through (5), it appears that a value of $\sigma_0^{(2)}/\sigma_R^{(2)}$ that is 5 or larger is sufficient to satisfy the requirement $|p/\sigma^{(2)}| \ll 1$ thereby making the simple formula (20) accurate. However, the accuracy of (20) is complicated by other aspects of the growth.

If T is regarded as the duration of the period at the operating temperature in each cycle, and the net growth of the undulation during the Nth thermal cycle is assumed to be approximately the same as it is for the first cycle, then the cumulative growth of the undulation after N thermal cycles is given by $\delta_f/\delta_0 = N\omega$, where $\omega \equiv (\delta/\delta_0)_{t=T}$ is the net growth for the first cycle. Under these assumptions, significant amplification of the initial undulation can occur in hundreds of cycles if $\sigma_0^{(2)}$ and T are both sufficiently large (c.f. Fig. 11).

Regarding δ_f/δ_0 as the cumulative growth of the undulation at the time of failure, the number of thermal cycles to failure is given by[5]

$$N = \frac{1}{\omega}\left(\frac{\delta_f}{\delta_0}\right) = \frac{1-(L^*/L)^2}{[1+T/t^*]^{\lambda}-1}\left(\frac{\delta_f}{\delta_0}\right), \tag{22}$$

where t^* is given by (19) and λ given by (21) is rewritten using (8) as

$$\lambda = \frac{4\sqrt{3}\pi a(n^{(2)})(1-\nu^{(2)})}{(n^{(2)}-1)}\frac{\sigma^{(3)3/2}}{E^{(2)}\sqrt{\bar{E}^{(3)}}}\left(\frac{L^*}{L}\right)\left[1-\left(\frac{L^*}{L}\right)^2\right], \tag{23a}$$

$$\lambda = -\frac{480\sqrt{3}\pi a(n^{(2)})(1-\nu^{(2)})}{(n^{(2)}-1)}\frac{\sigma^{(3)3/2}}{E^{(2)}\sqrt{\bar{E}^{(3)}}}, \tag{23b}$$

where the expression in (23b) has been evaluated at the critical value of the dimensionless wavelength for a single-cycle history, $L^*/L = 5$. The magnitude of the equi-biaxial stress in the bond coat at the beginning of the thermal cycle, $\sigma_0^{(2)}$, has a major influence on ω through t^*.

It is desirable to design the system such that N is as large as possible. It follows from (22) that N can be increased by increasing t^* or by decreasing λ. Increasing the creep reference stress of the bond

[5] If the stress in the oxide is compressive, i.e. $\mathrm{sgn}(\sigma_{11}^{(3)}) = -1$.

coat, $\sigma^{(2)}$, or decreasing the magnitude of the initial equi-biaxial stress in the bond coat, t^*, leads to an increase in t^*. The magnitude of the initial stress in the bond coat could be reduced by minimizing the effective thermal mismatch between the bond coat and the superalloy substrate. Reducing the magnitude of the compressive stress in the oxide layer (which results from lateral growth within the layer), $\sigma^{(3)}$, decreases λ. The parameter λ is small, thus $[1 + T/t^*]^{\lambda} - 1 \approx \lambda \ln(1 + T/t^*)$ from which it can be seen that halving λ doubles N whereas doubling t^* leads to a much smaller increase in N. This suggests that λ has the greatest effect on the lifetime of the thermal barrier system. Therefore, controlling the growth of the oxide stress, if possible, appears to be the most effective way to reduce undulation growth.

Undulation growth for a cyclic thermal history based on (15), (17) and (18), with the equi-biaxial stress in the bond coat renewed at the start of each cycle, is shown in Fig. 15 for five cycles, and in Fig. 16 for 100 cycles. Details of the heat-up and cool-down parts of the thermal history are not included in the present model. In both figures, $t_{cycle} = 1$ h, i.e. the system is held at the operating temperature for 1 h each cycle. In Fig. 15, the curve corresponding to $L_0^*/L = 3(h^{(3)}/L \approx 0.17)$ gives the greatest total undulation growth over five cycles whereas the greatest total growth for the 100 cycle simulation shown in Fig. 16 occurs for $L_0^*/L = 0.75(h^{(3)}/L \approx 0.04)$ which is close to the buckling wavelength $L_0^*/L = 1$. In each figure, the dashed curve is the prediction of the simple formula given by (20) for the wavelength that gives the greatest total growth. The simple formula provides a fairly good approximation of undulation growth for thermal histories with less than 50 cycles, but deviates from the complete analysis as the number of thermal cycles becomes large as shown in Fig. 16. For the parameters used in these simulations, the undulation can as much as double in size over the duration of the thermal history.[6]

Curves corresponding to values of L_0^*/L less than unity grow indefinitely, but slowly over the first 5–10 thermal cycles, whereas curves corresponding to values of L_0^*/L greater than unity grow more quickly during the first few thermal cycles

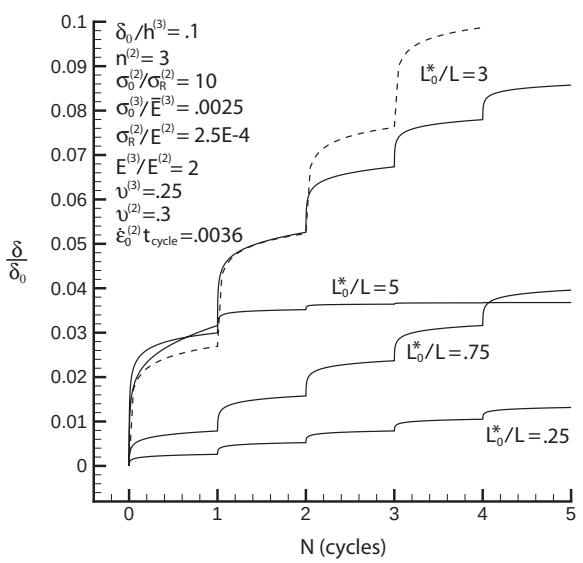

Fig. 15. Growth of the undulation for five thermal cycles where the system is held at the operating temperature for 1 h each cycle. The dashed curve is based on (20) and corresponds to $L_0^*/L = 3$.

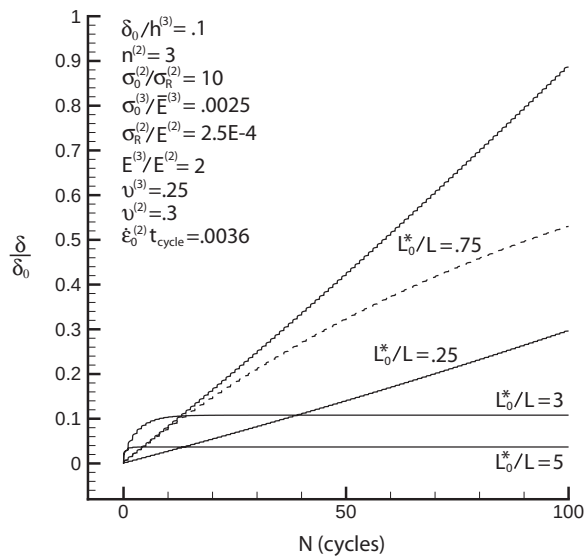

Fig. 16. Growth of the undulation for 100 thermal cycles where the system is held at the operating temperature for 1 h each cycle. The dashed curve is based on (20) and corresponds to $L_0^*/L = 0.75$.

[6] The analysis presented in this paper may lose accuracy as the undulation becomes large.

but eventually stop altogether. Shorter wavelengths initially grow more quickly because, for fixed δ_0, the magnitude of the normal traction at the oxide/bond coat interface at $t = 0$ decreases as the wavelength increases (the long wavelength limit is a perfectly planar film, which results in zero stress at the interface). Assuming the wavelength of the undulation remains fixed throughout the thermal history, these simulations suggest that the wavelength that gives the greatest total growth for a cyclic thermal history is largely dependent on the number of thermal cycles, and to a lesser degree, the duration of the isothermal period. However, further analysis is needed to determine if it is possible for longer wavelengths ($L_0^*/L \leq 1$) to survive the first few cycles, during which the shorter wavelengths ($L_0^*/L > 1$) are dominant.

Another possibility is supported by recent experimental results on FeCrAl bond coats which show that the wavelength of the undulation increases as the amplitude increases when the system is held at high temperature [14]. The analysis presented in this paper suggests that the value of L_0^*/L that gives the greatest growth decreases as the number of thermal cycles increases, as the results in Figs. 15 and 16 show. Using the same $h^{(3)}$ and $\sigma^{(3)}$ for each simulation, this corresponds to an increase in the undulation wavelength, $2L$, as the amplitude of the undulation, $\delta_0 + \delta$, increases. The undulation may spread as the amplitude increases so as to maximize the release of strain energy from the compressed oxide film during the period when the bond coat is highly susceptible to transverse deformation. An increase in wavelength would be inhibited by the zirconia top-layer. However, once fracture occurs in the top-layer parallel to and just outside the interface with the oxide, a tendency for the undulation to increase its wavelength could be a driving force for coalescence of cracks that are on the order of the undulation wavelength into a much larger delamination which could lead to widespread spallation.

A comparison of the 100-cycle thermal history shown in Fig. 16 with an isothermal history for the same total time exposure at the operating temperature is given in Fig. 17. Far more undulation growth occurs for the cyclic thermal history, about 65 times that of the isothermal history. After only

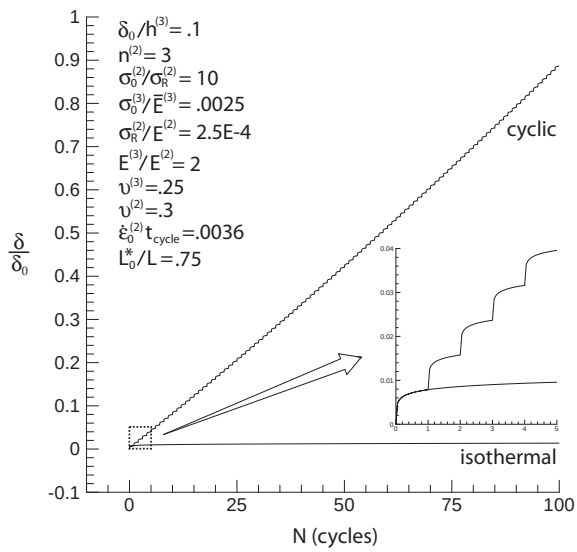

Fig. 17. Comparison of undulation growth for a cyclic thermal history with that of an isothermal history for the same total time exposure at the operating temperature. The inset shows an expanded view of the first five cycles. Far more undulation growth occurs for the cyclic thermal history, which is in agreement with experimental observations.

a few cycles, the undulation growth of the cyclic history is several times that of the isothermal history (c.f. inset, Fig. 17). This comparison indicates that the stress in the bond coat is essential to undulation growth. For a cyclic thermal history, the equi-biaxial compressive stress in the bond coat is renewed each cycle during the heat-up as a result of the phase transformation in the bond coat (c.f. Fig. 9). Conversely, the stress relaxes to zero and remains at zero thereafter for an isothermal history. Relaxation of the bond coat stress greatly enhances the creep resistance of the bond coat, making further undulation growth extremely difficult.

4. Concluding remarks

The main purpose of the specialized study in the present paper has been to reveal the importance of the nonlinear coupling between the equi-biaxial stress in the bond coat and the normal traction associated with undulations in the oxide film. Due to the transient nature of the equi-biaxial stress, there is a period of high susceptibility to undulation

growth at the beginning of each cycle. Eq. (13) governing the deformation of the bond coat can be used in models which incorporate more details of actual thermal barrier systems. These would include the effect of the porous ceramic top coat, yielding of the oxide film, the influence of oxide film growth on $\sigma^{(3)}$ and $h^{(3)}$, and the full specifics of the thermal history. In particular, simulations which produce the history of the equi-biaxial stress over the full history of heating and cooling are required for a better understanding of the levels of $\sigma_0^{(2)}/\sigma_R^{(2)}$ to be expected.

The time scale t^* in (19) corresponding to the decay of $\sigma^{(2)}$ is central to undulation growth. Increasing t^* decreases the net growth of the undulation for a fixed duration of the thermal cycle. By (19), t^* depends on the material properties of the bond coat and $\sigma_0^{(2)}$. As already remarked, decreasing $\sigma_0^{(2)}$ increases t^*, and $\sigma_0^{(2)}$ is related to the mismatch due to thermal expansion and the phase transformation in the bond coat. Increasing the reference creep stress, $\sigma_R^{(2)}$, has a strong effect since $t^* \propto \sigma_R^{(2)n}$. It is less clear how increasing $\sigma_R^{(2)}$ will alter $\sigma_0^{(2)}$, but there is likely to be a connection. The parameter λ in (23a,b) has an even stronger influence on undulation growth. Decreasing λ prolongs the life of the thermal barrier system. This can be accomplished by controlling the stress in the oxide layer, which appears to be the most effective way to reduce undulation growth.

Assuming the wavelength of the undulation is fixed, the value that gives the greatest total growth for a given thermal history depends on the number of thermal cycles and the duration of the period at the operating temperature. If, in an actual thermal barrier system, the current population of undulations at the oxide/bond coat interface could be surveyed using non-invasive techniques, the results of this model might be useful in predicting which undulations, based on their respective wavelengths, are more likely to lead to failure.

The results also suggest that an undulation that is finite in extent and far from any free edges might spread out as it grows, i.e. the wavelength of the undulation increases as the amplitude increases. An evolution from small to large wavelengths has been observed experimentally in some systems under isothermal conditions.

The strong nonlinear interaction between the stress in the bond coat and the normal traction that gives rise to undulation growth appears to be the explanation for the observation that undulation growth under cyclic thermal histories far exceeds that under isothermal conditions for the same total time exposure at the operating temperature. Simulations showed that undulation growth for a 100-cycle history with periods at the operating temperature lasting 1 h can be as much as 50–100 times that of an isothermal history with 100 h at the operating temperature.

In conclusion, the present work points to a number of avenues for continued research. Further progress will be possible by capitalizing on the solution for the bond coat given by (13), but simulations based on finite element modeling may also be required. The present model constitutes a framework to which further details of the thermal barrier system can be added. A revision of the model which incorporates the thermal barrier coating, growth of the oxide film, and yielding of the oxide film, is forthcoming. Simulations using the revised model will be performed for realistic full thermal histories and compared to finite element results, and the evolution of the undulation wavelength will be studied in detail.

Acknowledgment

This work was supported in part by the ONR MURI grant entitled “Prime Reliant Coatings” and in part by the Division of Engineering and Applied Sciences at Harvard University.

Appendix A

Solution for $a(n^{(2)})$ using a perturbation analysis

Consider a planar power-law layer that is in steady-state and under general biaxial stress, $\sigma_{11} \equiv \sigma_1$ in-plane and $\sigma_{33} \equiv \sigma_3$ out-of-plane. The layer is bonded to an infinitely thick substrate, and a sinusoidal normal traction is applied at the free

surface of magnitude $|p|$ and half-wavelength L where p is small relative to the effective stress that results from the biaxial stress (c.f. Fig. 3(b)). The deviatoric and effective stresses in the layer when $p = 0$ are

$$s^0_{11} = \frac{1}{3}(\sigma_3 - 2\sigma_1), \tag{A.1}$$

$$s^0_{22} = \frac{1}{3}(\sigma_1 + \sigma_3), \tag{A.2}$$

$$s^0_{33} = \frac{1}{3}(\sigma_1 - 2\sigma_3), \tag{A.3}$$

$$\sigma^0_e = \sqrt{\sigma_1^2 - \sigma_1\sigma_3 + \sigma_3^2}, \tag{A.4}$$

with σ_1 and σ_3 steadily maintained by straining of the underlying substrate. When p is nonzero, the deviatoric stress is given by

$$s_{ij} = s^0_{ij} + \eta\tilde{s}_{ij} + O(\eta^2), \tag{A.5}$$

where the perturbations $\tilde{s}_{ij}$ satisfy the equations of plane strain and the perturbation parameter $\eta = p/\sigma^0_e$ is small. The solution is obtained to first order in η thereby providing the plane strain stress perturbations.

The strain rates are given by

$$\dot{\varepsilon}_{ij} = \dot{\varepsilon}^0_{ij} + \eta\tilde{\dot{\varepsilon}}_{ij} + O(\eta^2), \tag{A.6}$$

where

$$\tilde{\dot{\varepsilon}}_{ij} = \frac{3}{2}\frac{\dot{\varepsilon}_R}{\sigma^n_R} \left[\sigma_e^{0^{n-1}}\tilde{s}_{ij} + \frac{3}{2}(n-1)\sigma_e^{0^{n-3}}s^0_{kl}\tilde{s}_{kl}s^0_{ij}\right]. \tag{A.7}$$

The plane strain compatibility equation for the strain rate perturbations is

$$\tilde{\dot{\varepsilon}}_{11,22} + \tilde{\dot{\varepsilon}}_{22,11} - 2\tilde{\dot{\varepsilon}}_{12,12} = 0. \tag{A.8}$$

Equilibrium, $\tilde{\sigma}_{\alpha\beta,\beta} = 0$, is satisfied by expressing the stress perturbations in terms of the usual Airy stress function using

$$\tilde{\sigma}_{11} = \frac{\partial^2\Phi}{\partial x_2^2},\ \tilde{\sigma}_{22} = \frac{\partial^2\Phi}{\partial x_1^2},\ \tilde{\sigma}_{12} = -\frac{\partial^2\Phi}{\partial x_1\partial x_2}. \tag{A.9}$$

One can then show that

$$\tilde{s}_{11} = \frac{2(1 + n(\sigma_3/\sigma_1)^2) - (1 + n)(\sigma_3/\sigma_1)}{3 + n + 4n(\sigma_3/\sigma_1)((\sigma_3/\sigma_1) - 1)} \left[\frac{\partial^2\Phi}{\partial x_2^2} - \frac{\partial^2\Phi}{\partial x_1^2}\right], \tag{A.10}$$

$$\tilde{s}_{22} = \frac{(3n-1)(\sigma_3/\sigma_1) - 2n(\sigma_3/\sigma_1)^2 - 1 - n}{3 + n + 4n(\sigma_3/\sigma_1)((\sigma_3/\sigma_1) - 1)} \left[\frac{\partial^2\Phi}{\partial x_2^2} - \frac{\partial^2\Phi}{\partial x_1^2}\right], \tag{A.11}$$

$$\tilde{s}_{12} = -\frac{\partial^2\Phi}{\partial x_1\partial x_2}. \tag{A.12}$$

Substituting these expressions for the stress perturbations into the equation for compatibility of the strain rates, using (A.7), gives

$$\frac{\partial^4\Phi}{\partial x_1^4} + \frac{\partial^4\Phi}{\partial x_2^4} + g(n,\sigma_3/\sigma_1)\frac{\partial^4\Phi}{\partial x_1^2\partial x_2^2} = 0, \tag{A.13}$$

where

$$g(n,\sigma_3/\sigma_1) = \frac{3 - n - 2n(\sigma_3/\sigma_1)(1 - (\sigma_3/\sigma_1))}{n(1 - (\sigma_3/\sigma_1)(1 - (\sigma_3/\sigma_1)))}, \tag{A.14}$$

which simplifies to the biharmonic equation when $n = 1$.

The governing equation admits a separable solution of the form

$$\Phi = e^{sx_2}\cos(\pi x_1/L), \tag{A.15}$$

that reduces (A.13) to the following quartic equation for s:

$$s^4 - g(n,\sigma_3/\sigma_1)\left(\frac{\pi}{L}\right)^2 s^2 + \left(\frac{\pi}{L}\right)^4 = 0, \tag{A.16}$$

which has the roots

$$s_{1,2,3,4} = \pm\frac{\pi}{\sqrt{2}L}\left[g(n,\sigma_3/\sigma_1) \pm i\sqrt{4 - g^2(n,\sigma_3/\sigma_1)}\right]^{1/2}, \tag{A.17}$$

where $4–g^2(n,\sigma_3/\sigma_1)$ is non-negative for all σ_3/σ_1 when $n \geq 1$. When $n = 1$, (A.17) reduces to the roots obtained from the classic solution of a sinusoidal load on an elastic half-space. In general, the roots can be expressed in complex notation as

$$s_{1,2,3,4} = \pm s_R \pm i\, s_I = \frac{\pi}{L}(\pm \cos(\theta/2) \pm i \sin(\theta/2)), \tag{A.18}$$

where

$$\theta = \tan^{-1}\left(\frac{\sqrt{4-g^2(n,\sigma_3/\sigma_1)}}{g(n,\sigma_3/\sigma_1)}\right) + m\pi, \tag{A.19}$$

and the integer m is needed to select the correct branch of the inverse tangent, where $\tan^{-1}$ is defined in the conventional way as the inverse of the principal branch of the tangent function. The value of m is equal to one when

$$n > 2 \quad \text{and} \quad \frac{-\sqrt{3}\sqrt{n-2} + \sqrt{n}}{2\sqrt{n}} < \frac{\sigma_3}{\sigma_1} < \frac{\sqrt{3}\sqrt{n-2} + \sqrt{n}}{2\sqrt{n}}, \tag{A.20}$$

and is otherwise zero. The general solution can be written as

$$\Phi = [(c_1 e^{s_R y} + c_2 e^{-s_R y})\cos(s_I x_2) + i(c_3 e^{s_R y} + c_4 e^{-s_R y})\sin(s_I x_2)]\cos(\pi x_1/L), \tag{A.21}$$

where the constants are in general complex. The argument $\theta/2$ is always positive and less than $\pi/2$, thus $\cos(\theta/2)$ is always positive. The stresses must be bounded as $x_2 \rightarrow -\infty$, which requires that c_2 and c_4 be zero. The solution must be real, thus c_1 is real and c_2 is imaginary.These conditions together with the traction boundary conditions

$$\eta\tilde{\sigma}_{12}(x_1,0) = 0, \tag{A.22}$$

$$\eta\tilde{\sigma}_{22}(x_1,0) = p\cos(\pi x_1/L), \tag{A.23}$$

lead to the solution for the stress function for $n > 1$

$$\frac{\Phi}{\sigma_e^0} = \left(\frac{L}{\pi}\right)^2 \cos\left(\frac{\pi x_1}{L}\right)\left[\cot(\theta/2)\sin\left(\sin(\theta/2)\frac{\pi x_2}{L}\right) - \cos\left(\sin(\theta/2)\frac{\pi x_2}{L}\right)\right] e^{\cos(\theta/2)(\pi x_2/L)} \tag{A.24}$$

The rate of change of the undulation amplitude is obtained from

$$\frac{\dot{\delta}}{L\dot{\varepsilon}_R} = \frac{\eta}{2}\int \Delta\left(\frac{\partial(\tilde{u}_2/\dot{\varepsilon}_R)}{\partial x_2}\right) d(x_2/L), \tag{A.25}$$

where Δ is used to signify the difference between the values at the peak and the valley of the undulation, and it follows from (A.7) and (A.10)–(A.12) that

$$\frac{\partial(\tilde{u}_2/\dot{\varepsilon}_R)}{\partial x_2} = \frac{3n}{3 + n - 4n(\sigma_3/\sigma_1)(1-(\sigma_3/\sigma_1))}\left(\frac{\sigma_e^0}{\sigma_R}\right)^n\left(\frac{\sigma_e^0}{\sigma_1}\right)^2\left(\frac{\partial^2(\Phi/\sigma_e^0)}{\partial x_1^2} - \frac{\partial^2(\Phi/\sigma_e^0)}{\partial x_2^2}\right). \tag{A.26}$$

Using the stress function given by (A.24), $\dot{\delta}$ simplifies to

$$\frac{\dot{\delta}}{L\dot{\varepsilon}_R} = \left(\frac{p}{\sigma_R}\right)\left(\frac{\sigma_e^0}{\sigma_R}\right)^{n-1} a(n,\sigma_3/\sigma_1), \tag{A.27}$$

where

$$a(n,\sigma_3/\sigma_1) = \frac{6n[1-(\sigma_3/\sigma_1)(1-(\sigma_3/\sigma_1))]\cos(\theta(n,\sigma_3/\sigma_1)/2)}{\pi[3 + n - 4n(\sigma_3/\sigma_1)(1-(\sigma_3/\sigma_1))]}, \tag{A.28}$$

and $\theta(n,\sigma_3/\sigma_1)$ is given by (A.19). When $n = 1$, the stress function differs from (A.24); however (A.27) and (A.28) are valid for $n \geq 1$. For an equibiaxial stress state, $\sigma_3/\sigma_1 = 1$, which gives

$$a(n) = \frac{6n}{\pi(3 + n)}\cos\left(\left(\tan^{-1}\left(\frac{\sqrt{3(n-1)(n + 3)}}{3-n}\right) + m\pi\right)/2\right), \tag{A.29}$$

and for plane strain, $\sigma_3/\sigma_1 = 1/2$, which gives

$$a(n) = \frac{3n}{2\pi}\cos\left(\left(\tan^{-1}\left(\frac{2\sqrt{n-1}}{2-n}\right) + m\pi\right)/2\right). \tag{A.30}$$

References

[1] Evans AG, Mumm DR, Hutchinson JW, Meier GH, Pettit FS. Progr Mat Sci 2001;46(5):505.

[2] He MY, Evans AG, Hutchinson JW. Mat Sci Eng 1998;A245:168.
[3] Sergo V, Clarke DR. J Am Ceram Soc 1998;3237:81.
[4] Wright PK, Evans AG. Curr Opin Sol State Phys 1999;4:255.
[5] Tolpygo VK, Clarke DR. Acta Mater 2000;48:3283.
[6] Evans AG, He MY, Hutchinson JW. Acta Mater 1997;45:3543.
[7] Mumm DR, Evans AG, Spitsberg IT. Acta Mater 2001;49:2329.
[8] He MY, Hutchinson JW, Evans AG. Acta Mater 2002;50:1063.
[9] Huang R, Suo Z. J Appl Phys 2002;91(3):1135.
[10] Karlsson AM, Hutchinson JW, Evans AG. J Mech Phys Solids 2002;50(8):1565.
[11] Karlsson AM, Hutchinson JW, Evans AG. Mat Sci Eng 2003;A351:244.
[12] Darzens S, Mumm DR, Clarke DR, Evans AG, Spitsberg IT. submitted for publication.
[13] Chen MW, Ott RT, Hufnagel TC, Wright PK, Hemker KJ. Surf Coat Technol 2003;163–164:25.
[14] Clarke DR. Private communication.